

PAPER • OPEN ACCESS

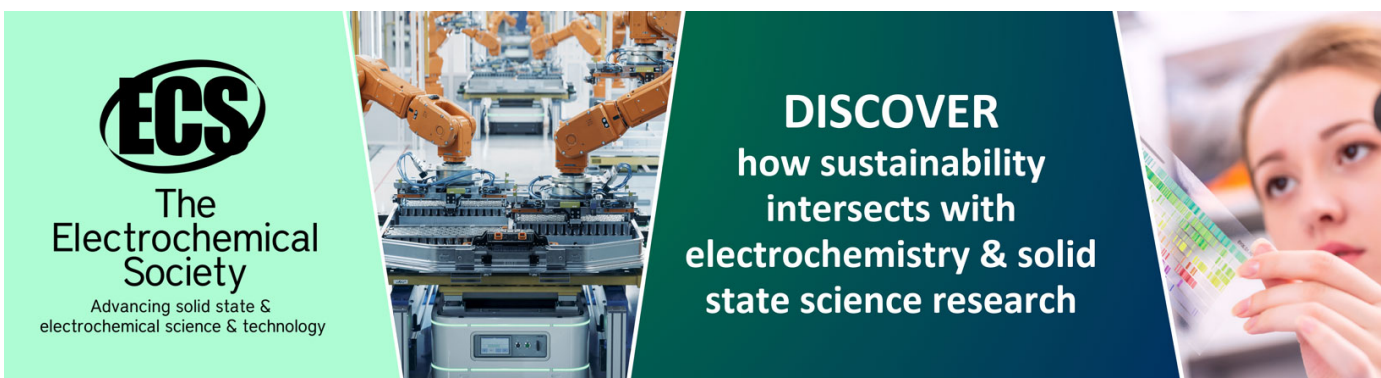
A Synaptic-plasticity Model Inspired by Metabolic Energy

To cite this article: Huanwen Chen and Lijuan Xie 2021 *J. Phys.: Conf. Ser.* **1746** 012009

View the [article online](#) for updates and enhancements.

You may also like

- [Inverse stochastic resonance in modular neural network with synaptic plasticity](#)
Yong-Tao Yu, , Xiao-Li Yang et al.
- [Improving the linearity of synaptic plasticity of single-walled carbon nanotube field-effect transistors via CdSe quantum dots decoration](#)
Yantao Zhang, Zhong Wang, Jia Liu et al.
- [W-doped In₂O₃ nanofiber optoelectronic neuromorphic transistors with synergistic synaptic plasticity](#)
Yang Yang, , Chuanyu Fu et al.



ECS
The
Electrochemical
Society
Advancing solid state &
electrochemical science & technology

DISCOVER
how sustainability
intersects with
electrochemistry & solid
state science research

A Synaptic-plasticity Model Inspired by Metabolic Energy

Huanwen Chen^{1,*} and Lijuan Xie²

¹School of Automation, Central South University, Changsha, China

²Institute of Physiological and Psychological Sciences, Changsha University of Science and Technology, Changsha, China

*Corresponding author email: hwchen@csu.edu.cn

Abstract. Inspired by the study of metabolic energy, a new synaptic plasticity model was established based on postsynaptic membrane potential and membrane current density. In this model, the change of synaptic weights is expressed by the difference between the resting energy state and firing energy state. The simulation results in L5 pyramidal neurons show that the proposed model can reproduce the triplet and quadruplet experiments of synaptic plasticity, which indicates that our model is feasible. The results of this paper will help to expand the synaptic plasticity model and the understanding of learning and memory from the perspective of energy.

Keywords: Homosynaptic plasticity; Neural Computation; Metabolic energy; Pyramidal neuron.

1. Introduction

The variables used by the traditional models of synaptic plasticity generally include pre and postsynaptic spike frequency^[1], pre and postsynaptic spike timing^[2], presynaptic spike and postsynaptic membrane potential^[3], and Ca^{2+} concentration^[4-5]. These models require presynaptic spike data directly or indirectly. It is not clear whether a model of synaptic plasticity can be established only by postsynaptic variables.

The human brain accounts for only 2% of the body's total weight, but consumes 20% of its resting metabolic energy^[6,7]. In addition to the costs associated with synaptic integration and transmission, experimental evidence suggests that synaptic plasticity itself is a costly process^[8-11]. Growing evidence suggests that metabolic energy may be a unifying principle governing neuronal activities^[12-15]. Thus, the study of synaptic plasticity from the perspective of metabolic energy has attracted more and more attention^[16]. Inspired by metabolic energy as a unified rule, we attempt to establish herein a model of synaptic plasticity based on postsynaptic membrane potential and membrane current density.

2. Synaptic Plasticity Model

Maintaining a constant transmembrane ion gradient is essential for neurons to function normally and even survive. Neurons have potential energy similar to batteries due to the existence of a transmembrane ion gradient^[14]. We call the potential energy of neurons in the resting state the resting energy state. Activities, such as action potential, input integration, and synaptic transmission, will change the potential energy of the neuron, leading to a new energy state, which is referred to as the firing energy state. To maintain normal information processing ability, neurons can restore the firing energy state to the resting energy state through active transport by expending metabolic energy. We assumed that synaptic plasticity might function similarly to, or be a manifestation of, active transport and be closely related to changes in the energy state of neurons. To restore the resting energy state,



when the firing energy state is larger than the resting energy state, the synaptic strength weakens, thus presenting as LTD. When the firing energy state is less than the resting energy state, the synaptic strength is enhanced, thus presenting as LTP. When the firing energy state is close to the resting energy state, the synaptic weight remains unchanged. The idea can be described by the following equation

$$W_j = A(E_j^r - E_j) \quad (1)$$

where W_j is the weight of synapse j , A is a scaling factor, E_j^r and E_j are the resting and firing energy states at the unit membrane of post-synapse j , respectively. E_j^r and E_j are all dimensionless variables. E_j represents the accumulated energy required when the membrane voltage is not below the firing threshold voltage, while E_j^r represents the accumulated energy when the membrane voltage is lower than the firing threshold voltage, so the two energy states can not be changed at the same time. When the membrane voltage is lower than the firing threshold voltage, E_j remains unchanged, while when the membrane voltage is higher than the firing threshold voltage, E_j^r remains unchanged. The differential expression of equation 1 is

$$\frac{dW_j}{dt} = A \left(\frac{dE_j^r}{dt} - \frac{dE_j}{dt} \right) \quad (2)$$

When the membrane voltage is lower than the firing threshold voltage, $\frac{dE_j}{dt} = 0$ because E_j remains unchanged. Similarly, when the membrane voltage is above the firing threshold voltage, $\frac{dE_j^r}{dt} = 0$ because E_j^r remains unchanged.

To calculate the energy states E_j^r and E_j in equations 1 and 2, one of the simplest and most straightforward methods is to describe the energy states by the product of postsynaptic membrane voltage v_m and postsynaptic membrane current density I_m . If the energy state needs to be restored to the resting state, the postsynaptic membrane voltage should reflect the difference between the intracellular potential and resting potential rather than the difference between the intracellular potential and extracellular potential expressed by v_m . Therefore, we defined a driving voltage $f_j(v_m)$ (figure 1a) to replace v_m .

$$f_j(v_m) = \text{sign}(v_m) |v_m - \theta_l| \quad (3)$$

where variable v_m is the postsynaptic voltage, θ_l is a parameter called the resting threshold voltage, v_m and θ_l are dimensionless with mV. In general, θ_l is less than the resting potential and larger than or equal to the minimum potential in pyramidal neurons. The direction of the driving voltage $f_j(v_m)$ is the same as that of v_m , and the amplitude is the absolute value of the difference between v_m and θ_l .

We also defined the driving current $g_j(I_m)$: when the postsynaptic membrane current density I_m does not exceed a certain threshold I_{max} , the driving current is equal to I_m , but when it exceeds I_{max} , the driving current decreases exponentially (figure 1b). To confer the homeostatic feature to our plasticity model^[17], we adopt the research results of intrinsic homeostatic plasticity for the design of the driving current^[18,19]. The idea of constructing a driving current is to make the functional relationship between $g_j(I_m)$ and I_m similar to figure 3c in Debane et al.^[18]. Electric power represents the change in energy per unit time; as such, the instantaneous change in the resting energy state and firing energy state in equation 2 ($\frac{dE_j^r}{dt}$ and $\frac{dE_j}{dt}$) can be expressed by the product of driving voltage and driving current.

To make our model homeostatic, we constructed the following driving current (figure 1b)

$$g_j(I_m) = \begin{cases} I_m, & |I_m| < I_{max} \\ I_{max} \text{sign}(I_m) \exp[D(I_{max} - |I_m|)], & |I_m| \geq I_{max} \end{cases} \quad (4)$$

where I_m is the current density at the postsynaptic membrane, I_{max} represents the maximum current density of the postsynaptic membrane, I_m and I_{max} are dimensionless with pA/ μm^2 . Parameter D denotes damping factor with $0 \leq D \leq 1$. If $|I_m| < I_{max}$, then the driving current $g_j(I_m)$ is equal to I_m ;

if $|I_m| \geq I_{max}$, then the amplitude of $g_j(I_m)$ decreases exponentially, consistent with the recent opinions^[18,19]. Equation 2 representing the change in synaptic strength over time with the driving voltage and driving current described above is as follows

$$\frac{dW_j}{dt} = A[\Theta(\theta_h - v_m)f_j(v_m)g_j(I_m) - \Theta(v_m - \theta_h)f_j(v_m)g_j(I_m)] \quad (5)$$

combined with the hard bounds $0.0002 \leq W_j/W_{ini} \leq 4$. Here W_{ini} is the initial weight. $\Theta(x)$ represents Heaviside function, $\Theta(x) = 1$ for $x \geq 0$ and $\Theta(x) = 0$ for $x < 0$. θ_h is called the firing threshold voltage, which is a dimensionless parameter with the unit of mV. $\Theta(\theta_h - v_m)f_j(v_m)g_j(I_m)$ is the time derivative term of the resting energy state, namely $\frac{dE_j^r}{dt}$ in equation 2. $\Theta(v_m - \theta_h)f_j(v_m)g_j(I_m)$ denotes the derivative of the firing energy state, that is $\frac{dE_j^f}{dt}$.

Equation 5 can now be used to more explicitly analyze the instantaneous synaptic strength change under different postsynaptic membrane voltage and membrane current density (figure 1c). $\Theta(v_m - \theta_h) = 0$ and $\Theta(v_m - \theta_h) = 1$ for $v_m \geq \theta_h$, thus equation 5 is reduced to $\frac{dW_j}{dt} = -Af_j(v_m)g_j(I_m)$. In this case, if the membrane voltage is in the same direction as the membrane current density, then the synaptic strength will decrease (S, T); otherwise, the synaptic strength will increase (E, F). On the other hand, if $v_m < \theta_h$, $\Theta(\theta_h - v_m) = 1$ and $\Theta(v_m - \theta_h) = 0$, then Equation (5) evolves into $\frac{dW_j}{dt} = Af_j(v_m)g_j(I_m)$. At this point, if the membrane voltage and membrane current density are in the same direction, then the synaptic strength increases (D); if they are in the opposite direction, then the synaptic strength decreases (R).

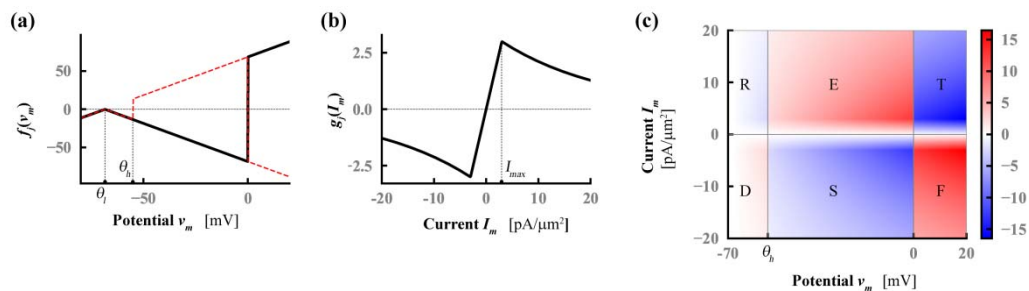


Figure 1. Illustration of the model.

(a) Relationship between postsynaptic membrane potential v_m and driving potential $f_j(v_m)$. The farther v_m was from the driving threshold potential θ_h , the larger the amplitude of the driving voltage (black solid line) would be, but $f_j(v_m)$ had the same sign as v_m . A transformation of the driving voltage (the dashed red line) stayed the same for $v_m < \theta_h$ and opposite sign occurred for $v_m \geq \theta_h$. (b) Relationship between postsynaptic membrane current density I_m and driving current $g_j(I_m)$. The amplitude of $g_j(I_m)$ decreased exponentially if the amplitude of I_m was larger than the allowable maximum current density I_{max} . (c) The instantaneous change in the synaptic strength under different postsynaptic membrane potential and membrane current density. The synaptic strength increased in D, E, and F but decreased in R, S, and T.

3. Reproduction of Triplet and Quadruplet Experiments

3.1. Model Parameters

In addition to the two variables of postsynaptic membrane voltage and postsynaptic membrane current density, our model includes five parameters: resting threshold voltage θ_l , maximum membrane current density I_{max} and damping factor D , scaling factor A and firing threshold voltage θ_\square . In the choice of model parameters, our goal is to make a set of parameters suitable for as many stimulation protocols as possible. The five model parameters are all determined by trial and error methods. The first is to

estimate the range of parameters according to their physical meaning, such as θ_l should be below -60 mV, θ_h should be between -60 and -50 mV, and so on. Then fine-tuning is done manually to make the simulation results match the experimental results as well as possible. We, therefore, simulated different parameters and determined four general model parameters by comparing the simulation results with the experimental data, that is, $A = 0.0625$, $\theta_l = -68.5$, $\theta_h = -55$ mV, $D = 0.05$, and $I_{max} = 3$ pA/ μm^2 .

All simulations in this paper were carried out on the Brian2 neuron simulator in Python^[20] based on the L5 pyramidal neuron models developed by Bono and Clopath^[21].

3.2. Triplet Protocol

Similar to the paired protocol, each distal and proximal compartment was connected to a synapse in the apical dendrite of the L5 pyramidal neuron (figure 2a). A current pulse of 1 nA lasting 3 ms was injected into the soma of postsynaptic neurons to induce a postsynaptic spike. The initial weight of all synapses was 0.5. To simulate the experimental protocol of Wang et al.^[22], the weight change was also multiplied by 12. The first triplet protocol (figure 2b) consisted of five sets of three spikes that were repeated at a given frequency of 1 Hz. Each triplet consisted of two presynaptic spikes and one postsynaptic spike. The time differences ($\Delta t_1, \Delta t_2$) were (5,-5), (10,-10), (15,-5), and (5,-15) respectively. The second triplet protocol (figure 2c) also included five sets of three spikes that repeated with a frequency of 1 Hz. The only difference from the first protocol was that each triplet consisted of a presynaptic spike and two postsynaptic spikes. The time differences between the two pairs ($\Delta t_1, \Delta t_2$) were set as (-5,5), (-10,10), (-5,15), and (-15,5).

3.3. Quadruplet Protocol

This protocol consisted of five quadruplets at a frequency of 1 Hz (figure 2d). A post-pre pair with a time difference of $\Delta t_1 = -5$ ms was followed by a pre-post pair with a time difference of $\Delta t_2 = 5$ ms after time T . In this case, T was set to positive. When T is negative, a pre-post pair with a time difference of $\Delta t_1 = 5$ ms was followed by a post-post pair with a time difference of $\Delta t_2 = -5$ ms after time T . Formally, T was defined by $T = \frac{(t_2^{pre} + t_2^{post})}{2} - \frac{(t_1^{pre} + t_1^{post})}{2}$. This protocol was repeated with various T (-100, -80, -60, -50, -40, -30, -25, -20, -15, -10, 10, 15, 20, 25, 30, 40, 50, 60, 80, 100).

3.4. Simulation Results

To prove the effectiveness of our model, we considered a hippocampal culture data set, which consists of triplet and quadruplet protocols (figure 2b,c). The mean weight of the proximal synapses in our model reproduces the triplet experimental results (figure 6c in Wang et al.^[22], Table 2 in Pfister and Gerstner^[2]), whereas the mean weight of the distal synapses is significantly different from the experimental results. In the triplet experiment of Wang et al.^[22], the location of the stimulus in the dendritic branch was not shown, while the simulation results of the proximal stimulation are quite consistent with the experimental results (figure 6c in Wang et al.^[22], table 2 in Pfister and Gerstner^[2]), so we judge that the stimulus location in the triplet experiment of Wang et al.^[22] is at the proximal site. In the quadruplet simulations (figure 2d), the average weight of all synapses at the proximal and distal ends of the dendritic branches can well fit the experimental results (figure 5 in Wang et al.^[22], table 2 in Pfister and Gerstner^[2]).

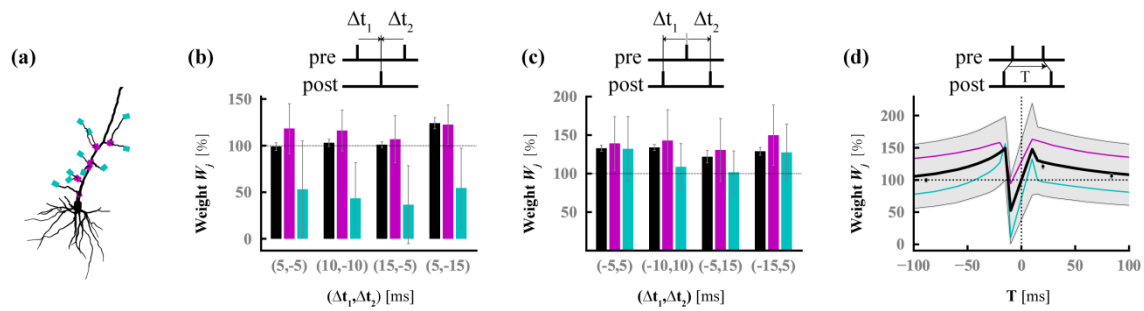


Figure 2 Reproducing the triplet and quadruplet experiments.

Each protocol was repeated 60 times with a frequency of 1Hz for apical compartments. Black bars and dots represented the experimental data from Wang et al.^[22] and table 2 in Pfister and Gerstner^[2]. Magenta bars: average synaptic weights for proximal compartments, cyan bars: average synaptic weights for distal compartments. (a) Proximal (magenta) and distal (cyan) locations on a thin apical branch of the detailed neuron model. (b) Synaptic strength changes corresponding to different time intervals under the four pre-post-pre protocols. Each protocol consisted of two presynaptic spikes and one postsynaptic spike characterized by $\Delta t_1 = t^{\text{post}} - t_1^{\text{pre}}$ and $\Delta t_2 = t^{\text{post}} - t_2^{\text{pre}}$ where t_1^{pre} and t_2^{pre} were the first and second presynaptic spikes of the triplet. (c) Synaptic strength changes corresponding to different time intervals under the four-post-pre-post protocols. Each protocol consisted of one presynaptic spike and two postsynaptic spikes. In this case, $\Delta t_1 = t_1^{\text{post}} - t^{\text{pre}}$ and $\Delta t_2 = t_2^{\text{post}} - t^{\text{pre}}$ where t_1^{post} and t_2^{post} were the first and second postsynaptic spikes of the triplet. (d) Synaptic weight change as a function of a delayed time T under the quadruplet protocol. Magenta line corresponded to the average synaptic weights of proximal compartments, cyan line corresponded to the average synaptic weights of distal compartments, and blackline corresponded to the average synaptic weights of all compartments. The gray shaded regions represented the standard deviation of synaptic strength for all compartments.

4. Conclusion

We proposed a synaptic plasticity model inspired by the metabolic energy of postsynaptic neurons. The model suggests that to ensure the survival and normal physiological function of neurons, their energy state should be maintained at a normal resting energy state level. Neurons recover to the resting state by the active transport mechanism. The active transport mechanism moves ions back across the neuronal membrane against their electrochemical gradients through ion pumps (e.g., sodium-potassium pump) distributed on the cell membrane, which needs to be driven directly by metabolic energy (e.g., by the hydrolysis of ATP). Synaptic plasticity is associated with the degree of deviation of energy states. If the firing energy state is larger than the resting energy state, then the synaptic strength weakens; if the firing energy state is less than the resting energy state, then the synaptic strength strengthens; and if the firing energy state is relatively close to the resting energy state, then the synaptic weight remains unchanged. Simulation indicates that our results are in good agreement with the experimental results of triplet and quadruple synaptic plasticity. Our study will help to expand the synaptic plasticity model and the understanding of learning and memory from the perspective of energy.

Our model has been tested in a single pyramidal neuron and the results show that the model is in good agreement with the experimental results. However, it is not clear whether the model can be extended to the dynamics research for neural networks. This is a key point of our future research work.

References

- [1] Bienenstock E L Cooper L N Munro P W 1982 Theory for the development of neuron selectivity: orientation specificity and binocular interaction in visual cortex *J Neurosci* vol 2 pp 32–48

- [2] Pfister J P Gerstner W 2006 Triplets of spikes in a model of spike timing-dependent plasticity *J Neurosci* vol 26 pp 9673–9682
- [3] Clopath C Büsing L Vasilaki E Gerstner W 2010 Connectivity reflects coding: a model of voltage-based STDP with homeostasis *Nat Neurosci* vol 13 pp 344–352
- [4] Shouval H Z Bear M F Cooper L N 2002 A unified model of NMDA receptor-dependent bidirectional synaptic plasticity *Proc Natl Acad Sci USA* vol 99 pp 10831–10836
- [5] Graupner M Brunel N 2012 Calcium-based plasticity model explains sensitivity of synaptic changes to spike pattern, rate, and dendritic location *Proc Natl Acad Sci USA* vol 109 pp 3991–3996
- [6] Attwell D Laughlin S B 2001 An energy budget for signaling in the grey matter of the brain *Journal of Cerebral Blood Flow & Metabolism* vol 21 pp 1133–1145
- [7] Harris J J Jolivet R Attwell D 2012 Synaptic energy use and supply *Neuron* vol 75 pp 762–777
- [8] Placais P Y Preat T 2013 To favor survival under food shortage, the brain disables costly memory *Science* vol 339 pp 440–442
- [9] Jaumann S Scudelari R Naug D 2013 Energetic cost of learning and memory can cause cognitive impairment in honeybees *Biology Letters* vol 9 Article ID 20130149
- [10] Placais P Y de Tredern É Scheunemann L et al 2017 Upregulated energy metabolism in the Drosophila mushroom body is the trigger for long-term memory *Nature Communications* vol 8 Article ID 11510
- [11] Karbowski J 2019 Metabolic constraints on synaptic learning and memory *Journal of Neurophysiology* vol 122 pp 1473–1490
- [12] Laughlin S B 2001 Energy as a constraint on the coding and processing of sensory information *Current Opinion Neurobiology* vol 11 pp 475–480
- [13] Niven J E Laughlin S B 2008 Energy limitation as a selective pressure on the evolution of sensory systems *Journal of Experimental Biology* vol 211 pp 1792–1804
- [14] Hasenstaub A Otte S Callaway E et al 2010 Metabolic cost as a unifying principle governing neuronal biophysics *Proceedings of The National Academy of Sciences of The United States of America* vol 107 pp 12329–12334
- [15] Yu L Yu Y 2017 Energy-efficient neural information processing in individual neurons and neuronal networks *Journal of Neuroscience Research* vol 95 pp 2253–2266
- [16] Li H L van Rossum M C W 2020 Energy efficient synaptic plasticity *eLife* vol 9 Article ID e50804
- [17] Turrigiano G G 2012 Homeostatic synaptic plasticity: Local and global mechanisms for stabilizing neuronal function *Cold Spring Harb Perspect Biol* vol 4 pp 1–18
- [18] Debanne D Inglebert Y Russier M 2019 Plasticity of intrinsic neuronal excitability *Curr Opin Neurobiol* vol 54 pp 73–82
- [19] Gasselín C Inglebert Y Ankri N Debanne D 2017 Plasticity of intrinsic excitability during LTD is mediated by bidirectional changes in h-channel activity *Sci Rep* vol 7 p 14418
- [20] Goodman D Brette R 2009 The Brian simulator *Front Neurosci* vol 3 pp 192–197
- [21] Bono J Clopath C 2017 Modeling somatic and dendritic spike mediated plasticity at the single neuron and network level *Nat Commun* vol 8 p 706
- [22] Wang H X Gerkin R C Nauen D W Bi G Q 2005 Coactivation and timing dependent integration of synaptic potentiation and depression *Nat Neurosci* vol 8 pp 187–193